Available at www.sciencedirect.com

ScienceDirect

journal homepage: www.elsevier.com/locate/he

Numerical study of heat and mass transfer in a plate methanol steam micro reformer with methanol catalytic combustor

Ching-Yi Hsueh [a], Hsin-Sen Chu [a,b], Wei-Mon Yan [c,*], Chiun-Hsun Chen [a]

[a] Department of Mechanical Engineering, National Chiao Tung University, Hsin-Chu 300, Taiwan, ROC
[b] Industrial Technology Research Institute, Chu-Tung, Hsin-Chu 310, Taiwan, ROC
[c] Department of Greenergy, National University of Tainan, Tainan 700, Taiwan, ROC

ARTICLE INFO

Article history:
Received 16 December 2009
Received in revised form
1 March 2010
Accepted 7 March 2010
Available online 24 April 2010

Keywords:
Micro reformer
Catalytic combustor
Methanol
Numerical analysis

ABSTRACT

A numerical study is performed to examine the characteristics of heat and mass transfer and the performance of a plate methanol steam micro reformer with a methanol catalytic combustor. The effects of the flow configurations for co- and counter-current flows are explored in the present study. The influences of the Reynolds number (Re) and various geometric parameters on heat and mass transfer phenomena in the channels are also investigated numerically. It is expected that the Reynolds number (Re) and various geometric parameters can be improved by thermal management to enhance the chemical reaction and thus augment the micro reformer performance. Comparing the co- and counter-current flows via numerical simulation, the results show that the methanol conversion for counter-current flow could be improved by 10%. This is due to the fact that counter-current flow leads to a better thermal management, which in turn improves fuel conversion efficiency. With a higher Reynolds number on the combustor side, the wall temperature is increased and the methanol conversion can thus be enhanced. Meanwhile, a reduced Reynolds number on the micro reformer side would increase the methanol conversion. The results also reveal that appropriate geometric parameters exist for a micro reformer with a combustor to obtain better thermal management and methanol conversion.

1. Introduction

The proton exchange membrane fuel cell (PEMFC) is a promising alternative energy source due to the characteristics of high energy density, low noise and low pollution. Applications of PEMFC in portable power sources need to carry enough hydrogen fuel. However, the hydrogen storage problem is still difficult to overcome. To solve this technical difficulty, one possible solution is to employ a reformer. Methanol clearly has distinct advantages as a fuel for fuel cell applications due to its higher hydrogen-to-carbon ratio, low reforming temperature and greater environmental friendliness [1]. The PEMFC generates electronic energy using hydrogen produced by the reformer from methanol. Therefore, the methanol steam micro reformer with small PEMFC has become a potential candidate for portable electronic products in the near future.

There have appeared a number of experiments on the plate methanol steam micro reformer in the published literature. The micro reformer for methanol steam reforming was

* *Corresponding author*. Tel.: +886 6 260 2251; fax: +886 6 260 2205.
E-mail address: wmyan@mail.nutn.edu.tw (W.-M. Yan).
0360-3199/$ – see front matter © 2010 Professor T. Nejat Veziroglu. Published by Elsevier Ltd. All rights reserved.
doi:10.1016/j.ijhydene.2010.03.036

Nomenclature

C_i	concentration of species i (mol m^{-3})
c_p	specific heat at constant pressure (J kg^{-1} K^{-1})
D	hydraulic diameter (m)
D_{eff}	effective mass diffusivity (m^2 s^{-1})
D_k	mass diffusion coefficient (m^2 s^{-1})
D_p	catalyst particle diameter (m)
E_a	activation energy (J mol^{-1})
H	channel height (m)
H_C	combustion flow channel (m)
H_R	reforming flow channel (m)
H_w	solid wall thickness (m)
ΔH	enthalpy of reaction (J mol^{-1})
I, J, K	grid points in the x-, y- and z-directions, respectively
k_{eff}	effective thermal conductivity (W m^{-1} K^{-1})
k_f	fluid phase thermal conductivity (W m^{-1} K^{-1})
k_p	permeability (m^2)
k_s	solid medium thermal conductivity (W m^{-1} K^{-1})
k_1	pre-exponential factor for steam reforming
k_2	pre-exponential factor for the reverse water-gas shift
k_3	pre-exponential factor for decomposition reaction
k_4	pre-exponential factor for combustion reaction
L	flow channel length (m)
M_i	mole fraction of species i
$M_{w,i}$	molecular weight of species i (kg mol^{-1})
p	pressure (Pa)
R	universal gas constant
R_{SR}	Arrhenius reaction rate coefficient for steam reforming (mol m^{-3} s^{-1})
R_{rWSG}	Arrhenius reaction rate coefficient for the reverse water-gas shift (mol m^{-3} s^{-1})
R_{MD}	Arrhenius reaction rate coefficient for decomposition reaction (mol m^{-3} s^{-1})
$R_{Combustion}$	Arrhenius reaction rate coefficient for combustion reaction (mol m^{-3} s^{-1})
Re	Reynolds number, $Re = \rho u D/\mu$
T	temperature (°C)
T_0	inlet temperature (°C)
T_w	wall temperature (°C)
u, v, w	velocity components in the x-, y- and z-directions, respectively, (m s^{-1})
$u_{0,C}$	inlet flow velocity on the combustion channel side (m s^{-1})
γ	dimensionless coordinate, $\gamma = y/H_C + \delta_c + H_W + H_R + \delta_R$
x, y, z	coordinates (m)
W_R	channel width (m)
W_L	steel width (m)

Greek symbols

δ_C	combustion catalyst layer thickness (m)
δ_R	reforming catalyst layer thickness (m)
ε	porosity
η	methanol conversion
τ	tortuosity of the porous medium
μ	viscosity (kg m^{-1} s^{-1})
ρ	density (kg m^{-3})
ρ_s	catalyst density (kg m^{-3})

Subscripts

eff	effective
u	x-direction
v	y-direction
w	z-direction
0	inlet

designed to produce hydrogen for small PEMFCs. As the steam reforming reaction is an endothermic reaction, electric heaters to provide heat for the steam reforming were used by several investigators [2–7]. The plate integrated fuel processor, consisting of various micro structured modules, was developed to produce hydrogen for fuel cell systems. The fuel processor includes a fuel vaporizer, a catalytic combustor and a steam reformer. The catalytic combustor supplied heat to the steam reforming reaction, and the hydrogen was produced by the micro methanol steam reformer [8–15]. For the PEM fuel cell, the CO concentration must be less than 10 ppm, so a cleanup step is required after methanol steam reforming. The integration of the PrOx or water-gas shift reaction equipment to reduce the CO concentration in the gas from the methanol steam reformer has been used by several researchers [16,17].

To reduce the research cost and shorten the design cycle, modeling and simulation are being used extensively in research institutions and industries across the world to gain a better understanding of the fundamental processes in a methanol steam reformer. Therefore, a vast amount of literature has been focused on theoretical modeling of the methanol steam reformer. Several articles have employed a cylindrical mathematical model of a packed bed reformer to investigate heat and mass transport phenomena in a methanol reformer [18–23]. A numerical plate micro reformer model to analyze the micro reformer performance and reactant gas transport characteristics was presented by several investigators [24–29].

The systems are fed by hydrocarbons which convert hydrogen and generate heat, and studies have developed numerical models of a micro reformer with a combustor to explore the heat and mass transport phenomena and fuel conversion efficiency. Deshmukh and Vlachos [30,31] presented a two-dimensional model of propane (C_3H_8) combustion with ammonia (NH_3) decomposition to investigate micro reactors for hydrogen production. The results show that the H_2 production rate and the temperatures generated via the C_3H_8 combustion both increase as the flow rate of ammonia increases. The results also show that the co-current flow configuration has a lower reactor temperature and allows a wider spectrum of materials to be used than the counter-current flow configuration. A microchannel model of the thermal integration of a steam reformer and a catalytic combustor was established by Arzamendi and collaborators [32,33]. Using the hydrogen produced by the reforming reaction from methanol and methane, the results

showed the short diffusion distance and higher area to volume ratio required for using the micro reactor. The results also indicated that complete combustion of methane takes place over a very short distance. The reforming fuel is rapidly heated and then the methane reactor has a more uniform temperature distribution. Pan and Wang [34] designed a plate-fin reformer which integrated endothermic and exothermic reactions into one unit. The combustor supplied the heat for the methanol steam reformer. Their numerical model accurately predicted the methanol conversion rate and the gas distributions. A two-dimensional model of a plate methane reformer with methane combustor to investigate thermo-fluid parameters and geometric parameters was developed by Zanfir and Gavriilidis [35]. Their results showed that the micro reformers have better performance than traditional reformers due to their better heat and mass transfer. The results also showed that a higher channel height produces a lower conversion and much more uniform temperature distribution. Varesano et al. [36] used a one-dimensional transient mathematical model to study the transport behavior in a steam reforming reactor with a burner that supplies heat.

From the literature survey presented above, it was found that some literature is available on mathematical models of the methanol steam micro reformer, but little information is available on mathematical models of a micro reformer with a catalytic combustor. Therefore, the objective of the present study is to investigate the transport phenomena and the fuel conversion efficiency in a methanol steam micro reformer with methanol catalytic combustor. A three-dimensional numerical model of a micro reformer with combustor is developed to examine the effects of various flow configurations and geometric parameters on micro reformer performance.

2. Analysis

The reactor consists of a methanol steam micro reformer and a methanol catalytic combustion chamber. A schematic diagram of the physical system under consideration is shown in Fig. 1. The system consists of a solid wall, two catalyst layers and two flow channels each at the catalytic combustion/steam reforming side. It is seen that the methanol catalytic combustion chamber and the methanol steam reforming chamber are separated by a solid wall. Both sides of each channel are coated with a combustion catalyst layer and a steam reforming catalyst layer. The heat from the combustion reaction is used to drive the steam reforming reaction. To simplify the analysis for the present study, the flowing assumptions are made:

(1) the flow is steady state;
(2) the inlet fuel is an ideal gas;
(3) the flow is laminar and incompressible;
(4) the catalyst layer is isotropic;
(5) the chemical reaction occurs only in the catalyst layer;
(6) thermal radiation and conduction in the gas phase are negligible compared to convection.

With the above assumptions, the gas transport equations for the three-dimensional reactor can be described as follows. Continuity equation:

$$\rho\left(\frac{\partial u}{\partial x}+\frac{\partial v}{\partial y}+\frac{\partial w}{\partial z}\right)=0 \tag{1}$$

X-momentum equation:

$$\varepsilon\rho\left(u\frac{\partial u}{\partial x}+v\frac{\partial u}{\partial y}+w\frac{\partial u}{\partial z}\right)=-\varepsilon\frac{\partial p}{\partial x}+\varepsilon\mu\left(\frac{\partial^2 u}{\partial x^2}+\frac{\partial^2 u}{\partial y^2}+\frac{\partial^2 u}{\partial z^2}\right)+S_u \tag{2}$$

Y-momentum equation:

$$\varepsilon\rho\left(u\frac{\partial v}{\partial x}+v\frac{\partial v}{\partial y}+w\frac{\partial v}{\partial z}\right)=-\varepsilon\frac{\partial p}{\partial y}+\varepsilon\mu\left(\frac{\partial^2 v}{\partial x^2}+\frac{\partial^2 v}{\partial y^2}+\frac{\partial^2 v}{\partial z^2}\right)+S_v \tag{3}$$

Z-momentum equation:

$$\varepsilon\rho\left(u\frac{\partial w}{\partial x}+v\frac{\partial w}{\partial y}+w\frac{\partial w}{\partial z}\right)=-\varepsilon\frac{\partial p}{\partial z}+\varepsilon\mu\left(\frac{\partial^2 w}{\partial x^2}+\frac{\partial^2 w}{\partial y^2}+\frac{\partial^2 w}{\partial z^2}\right)+S_w \tag{4}$$

In the above equations, ϵ stands for the porosity of the medium, and the mixture viscosity μ_{mix} based on kinetic theory is [37]

$$\mu_{mix}=\sum_{i=1}^{5}\frac{M_i\mu_i}{\sum_{j=1}^{5}M_j\phi_{ij}} \tag{5}$$

where

$$\phi_{ij}=\sum_i\frac{\left[1+\left(\frac{\mu_i}{\mu_j}\right)^{\frac{1}{2}}\left(\frac{M_{w,j}}{M_{w,i}}\right)^{\frac{1}{4}}\right]^2}{\left[8\left(1+\frac{M_{w,i}}{M_{w,j}}\right)\right]^{\frac{1}{2}}} \tag{6}$$

S_u, S_v and S_w are corrected terms of the reactant gas flow in a porous material in the catalyst layer. The source terms, S_u, S_v and S_w in the momentum equations are listed in Eqs. (7–9), respectively. Among them, the source terms, S_u, S_v and S_w account for the Ergun equations [38] in the x-, y- and z-directions, respectively. The parameter k_p stands for the permeability and β is the inertial loss coefficient in each component direction.

$$S_u=-\frac{\mu u}{k_p}-\frac{\beta u\rho}{2}\sqrt{u^2+v^2+w^2} \tag{7}$$

$$S_v=-\frac{\mu v}{k_p}-\frac{\beta v\rho}{2}\sqrt{u^2+v^2+w^2} \tag{8}$$

$$S_w=-\frac{\mu w}{k_p}-\frac{\beta w\rho}{2}\sqrt{u^2+v^2+w^2} \tag{9}$$

where

$$k_p=\frac{D_p\varepsilon^3}{150(1-\varepsilon)^2} \tag{10}$$

$$\beta=\frac{3.5(1-\varepsilon)}{D_p\varepsilon^3} \tag{11}$$

and where D_p is the catalyst particle diameter.

Species equation:

$$\left(u\frac{\partial m_i}{\partial x}+v\frac{\partial m_i}{\partial y}+w\frac{\partial m_i}{\partial z}\right)=D_{eff}\left(\frac{\partial^2 m_i}{\partial x^2}+\frac{\partial^2 m_i}{\partial y^2}+\frac{\partial^2 m_i}{\partial z^2}\right)+(1-\varepsilon)\rho_s S_c \tag{12}$$

In the species equation, m_i denotes the mass fraction of the ith species, where the various species are CH_3OH, H_2O, H_2, CO_2, CO and O_2. In these expressions, the concentrations of

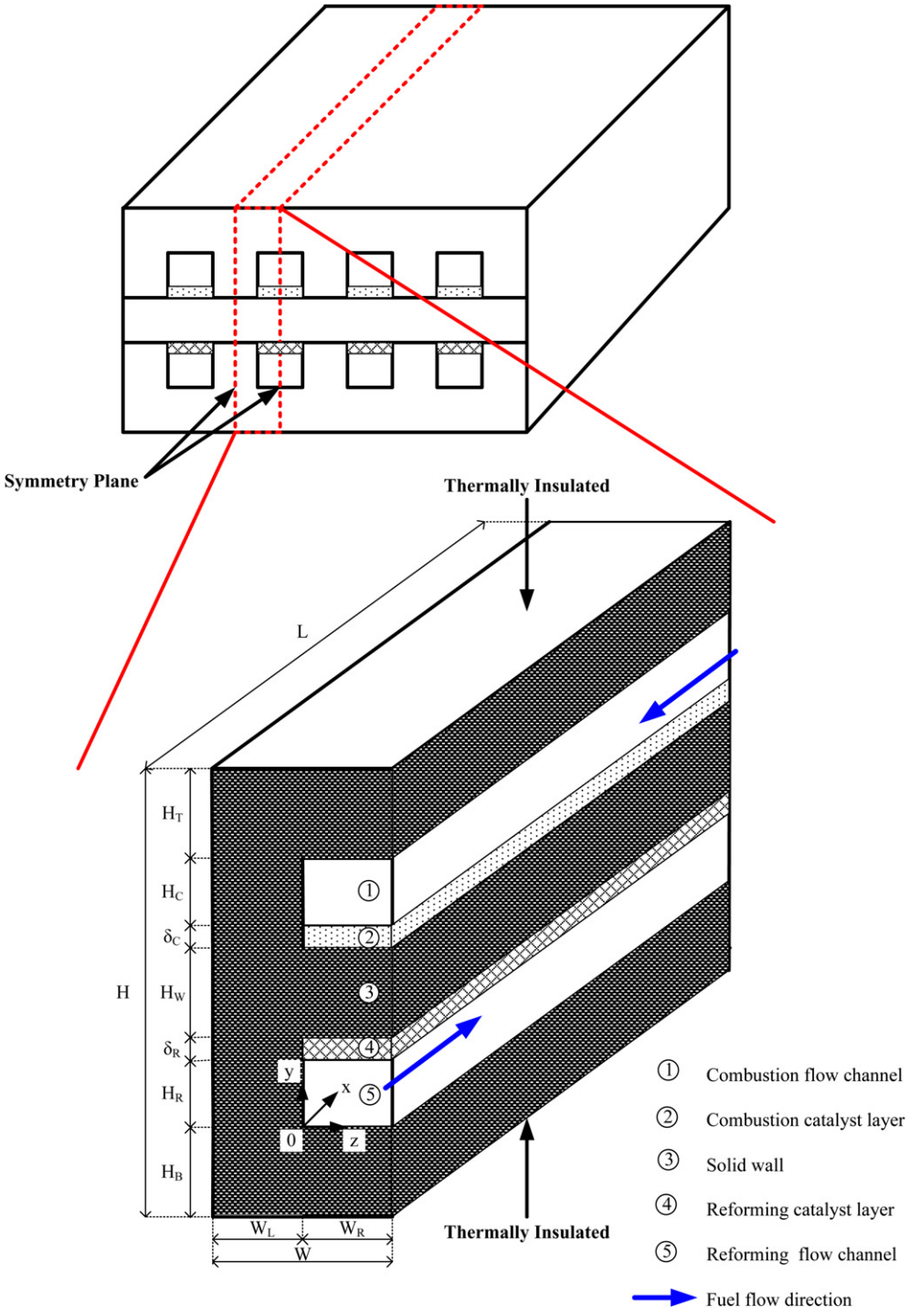

Fig. 1 – Schematic diagram of the present study.

CH_3OH, H_2O, H_2, CO_2, CO are calculated on the steam reforming side and CH_3OH, H_2O, CO_2, O_2 are calculated on the combustion side. The effective diffusion coefficient, D_{eff} is determined by the Stefan–Maxwell equations [37]. Eq. (13) is employed to describe the influence of the porosity on the diffusion coefficient:

$$D_{eff} = D_k \varepsilon^{\tau} \tag{13}$$

The diffusion coefficient D_k for the methanol steam micro reformer was derived from the Stefan–Maxwell equations which were used to calculate the mean effective binary diffusivity [21]. S_c is the source term of chemical reaction in the species equation, and differs according to the reactant gases in the catalyst layer. In the present study, there is no chemical reaction in the flow channel. Therefore, S_c is zero in the flow channel. In the catalyst layer, the source term of the

species equation, S_c, can be described by the following modified concentration term:

$$S_c = \begin{cases} M_{w,i}(R_{SR} + R_{rWGS} + R_{MD})(\lambda_i'' - \lambda_i') & \text{for steam reforming} \\ M_{w,i}(R_{Combustion})(\lambda_i'' - \lambda_i') & \text{for combustion reaction} \end{cases} \quad (14)$$

where $M_{w,i}$ is the molecular weight of species i, and $R_{i,r}$ is the Arrhenius molar rate of creation and destruction of species i in the reaction. λ_i'' and λ_i' are the stoichiometric coefficient for reaction i and product i, respectively, in the reaction.

According to the chemical kinetics of Pepply et al. [39], the methanol steam reforming reaction consists of three overall reactions: one is a primary process in methanol steam reforming and the others are the decomposition reaction and water-gas shift reaction. Therefore, the steam reforming reaction, Eq. (15), the reverse water-gas shift reaction, Eq. (16), and the decomposition reaction, Eq. (17), are considered in this study.

$$CH_3OH + H_2O \underset{k_{-1}}{\overset{k_1}{\leftrightarrow}} CO_2 + 3H_2 \quad (15)$$

$$CO_2 + H_2 \underset{k_{-2}}{\overset{k_2}{\leftrightarrow}} CO + H_2O \quad (16)$$

$$CH_3OH \overset{k_3}{\rightarrow} CO + 2H_2 \quad (17)$$

In this work, to simplify the analysis, the model of Mastalir et al. [40] for methanol steam reforming is used, and the Arrhenius equation is employed to calculate the reactant gases generated by the chemical reaction.

$$R_{SR} = k_1 C_{CH_3OH}^{0.6} C_{H_2O}^{0.4} \exp\left(-\frac{E_a}{RT}\right) - k_{-1} C_{CO_2} C_{H_2} \exp\left(-\frac{E_a}{RT}\right) \quad (18)$$

$$R_{rWGS} = k_2 C_{CO_2} C_{H_2} \exp\left(-\frac{E_a}{RT}\right) - k_{-2} C_{CO} C_{H_2O} \exp\left(-\frac{E_a}{RT}\right) \quad (19)$$

$$R_{MD} = k_3 C_{CH_3OH}^{1.3} \exp\left(-\frac{E_a}{RT}\right) \quad (20)$$

where the steam reforming reaction and reverse water-gas shift reaction are reversible reactions and the decomposition reaction is a non-reversible reaction. The constants k_1, k_2 and k_3 are forward rate constants, and the constant k_{-1} and k_{-2} are the backward rate constants.

The reaction of the combustion catalyst layer can be represented by the following reaction, Eq. (21). The reaction rate of methanol over the Pt/Al_2O_3 catalyst was calculated with Eq. (22), as proposed by Pasel et al. [41]

$$CH_3OH + 1.5O_2 \overset{k_4}{\rightarrow} CO_2 + 2H_2O \quad (21)$$

$$R_{Combustion} = k_4 C_{CH_3OH}^{1.3} \exp\left(-\frac{E_a}{RT}\right) \quad (22)$$

In order to evaluate the distributions of the local temperature, the energy equations must be solved.Energy equation:

$$\rho c_p \left(u\frac{\partial T}{\partial x} + v\frac{\partial T}{\partial y} + w\frac{\partial T}{\partial z}\right) = k_{eff}\left(\frac{\partial^2 T}{\partial x^2} + \frac{\partial^2 T}{\partial y^2} + \frac{\partial^2 T}{\partial z^2}\right) + (1-\varepsilon)\rho_s S_t \quad (23)$$

The effective thermal conductivity is modified to account for the porous medium effect:

$$k_{eff} = \varepsilon k_f + (1-\varepsilon)k_s \quad (24)$$

where k_f is the fluid phase thermal conductivity, k_s is the solid medium thermal conductivity and ϵ is the porosity of the medium.

The source term S_t in the energy equation due to the chemical reactions is determined by

$$S_t = \begin{cases} -(\Delta H_{SR} R_{SR} + \Delta H_{rWGS} R_{rWGS} + \Delta H_{MD} R_{MD}) & \text{for steam reforming} \\ -(\Delta H_{Combustion} R_{Combustion}) & \text{for combustion reaction} \end{cases} \quad (25)$$

As for the energy equation of the solid wall, one has

$$\frac{\partial^2 T}{\partial x^2} + \frac{\partial^2 T}{\partial y^2} + \frac{\partial^2 T}{\partial z^2} = 0 \quad (26)$$

The boundary conditions of the present computation include those at the inlet, the outlet, the wall, and the interface between the flow channel and the catalyst layer.

(1) The boundary conditions for inlets at the flow channel and the catalyst layer: the inlet flow velocity is constant, the inlet gas composition is constant, and the inlet temperature is constant.
(2) The boundary conditions for outlets at the flow channel and the catalyst layer: there is fully developed flow.
(3) The boundary conditions for the interface between the solid wall and the insulated walls: the temperature gradients are zero.
(4) The boundary conditions for the interface between the flow channel and solid wall: no slip and zero fluxes hold the velocities and the concentration gradients are zero.
(5) The boundary conditions for the interface between the flow channel and the catalyst layer: the velocities, temperatures, species concentrations and species fluxes are continuous.

The geometrical dimensions and parameters used are listed in Table 1.

3. Numerical method

The solution to the governing equations is found by employing a finite volume scheme with the model domain divided into a number of cells as control volumes. The governing equations are numerically integrated over each of these computational cells or control volumes. The method exploits a collocated cell-centered variable arrangement with the local or cell-averaged values of the physical quantities evaluated and stored at each cell center.

The governing equations can be expressed in the form of a generalized convection–diffusion type of transport equation:

$$\nabla \cdot (\rho \phi V) = \nabla \cdot (\Gamma \nabla \phi) + S_\phi \quad (27)$$

where ϕ is a general dependent variable, V is the velocity

Table 1 – Parameters used in this study.

Flow channel length L (m)	4×10^{-3}
Combustion catalyst layer thickness δ_C (m)	5.0×10^{-5}
Reforming catalyst layer thickness δ_R (m)	5.0×10^{-5}
Combustion flow channel H_C (m)	4.5×10^{-4}
Reforming flow channel H_R (m)	4.5×10^{-4}
Average inlet temperature (°C)	120
Operating pressure (atm)	1
Catalyst density (kg m^{-3}) [21]	1480
Catalyst thermal conductivity (W m^{-1} K^{-1}) [21]	0.3
Catalyst layer porosity [24]	0.38
Catalyst permeability (m^2) [24]	2.379×10^{-12}
Mass diffusion coefficient (m^2 s^{-1}) [21]	6.8×10^{-5}
Activation energy for steam reforming (J mol^{-1}) [40]	1.09×10^5
Activation energy for the reverse water-gas shift (J mol^{-1}) [40]	1.15×10^5
Activation energy for decomposition reaction (J mol^{-1}) [40]	1.42×10^5
Activation energy for combustion reaction (J mol^{-1}) [41]	1.3×10^4

vector, S_ϕ is the source per unit volume and ρ is the density. With the discretization of the governing equations, the coupled finite-difference equations become

$$a_P\phi_P = a_E\phi_E + a_W\phi_W + a_N\phi_N + a_S\phi_S + S_\phi \quad (28)$$

where ϕ_P is the value of ϕ at the current point P, $\phi_E \ldots \phi_S$ stand for the values of the grid points adjacent to the point P, and $a_P \ldots a_S$ are known as the link coefficients. All equations were numerically solved using the commercial fluid dynamics program Fluent™. The SIMPLE algorithm was employed to solve the convection–diffusion equations. The convergence criteria for the normalized residuals for each variable were restricted to less than 10^{-6}.

In this work, a grid system of $121 \times 81 \times 21$ points was used. To examine the grid independence of the predictions, three grid systems were considered and their influences on the prediction of local temperature distributions for a typical case are presented in Table 2. It is found that the maximum deviation among the computations using grids of $101 \times 62 \times 11$, $121 \times 81 \times 21$ and $141 \times 100 \times 31$ is less than 1.3% and the results on the $121 \times 81 \times 21$ and the $141 \times 100 \times 31$ grids are quite close. Therefore, the grid system of $121 \times 81 \times 21$ points seems sufficient to resolve the behaviors of local temperature distributions in the present micro reformer model. To further check the adequacy of the numerical scheme, it is clearly seen from Fig. 2 that the present predictions agree reasonably well with the experimental data of Won [10]. The above preliminary runs confirm that the present model and the numerical method used are generally appropriate for the analysis of the problem.

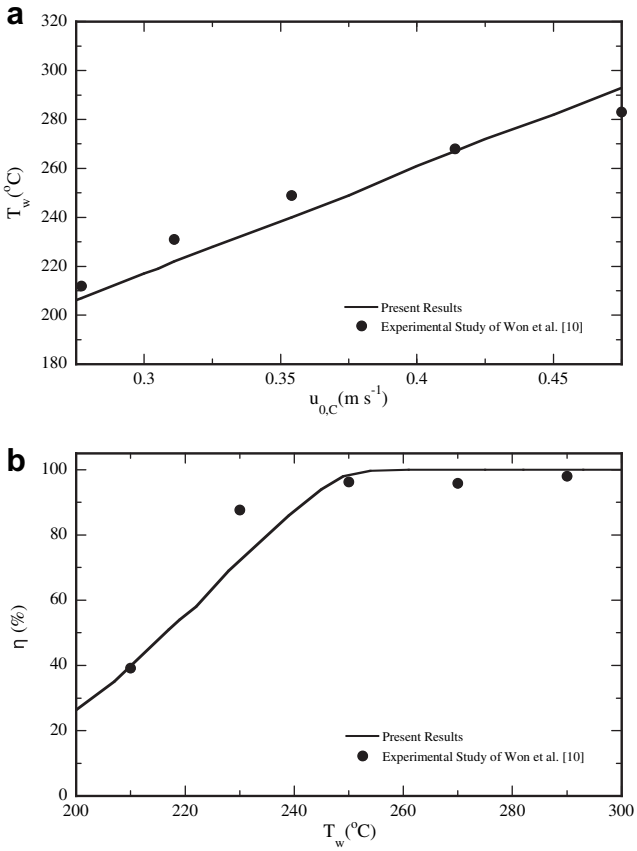

Fig. 2 – Comparison of theoretical simulation of the present results with previous experimental data by Won et al. [10].

4. Results and discussion

In the present paper, a three-dimensional model is analyzed to understand heat and mass transfer in the channels of a methanol steam micro reformer with methanol catalytic combustor. The influences of wall conduction effects on the transport phenomena of heat and mass transfer in a micro reformer with combustor are important. Therefore, the local temperature distributions along the centerline of the top reforming channel ($Y = 0.333$) and the CH_3OH mole fraction distributions along the centerline of the reforming channel ($Y = 0.167$) are presented in Fig. 3. In this work, X denotes the dimensionless distance from the flow channel inlet to the outlet. It is clearly seen in Fig. 3(a) that the temperature distributions with the wall thermal conduction effect show a lower and more uniform distribution than that without a wall conduction effect. This implies that the effects of wall

Table 2 – Temperature distributions (°C) for the various grid tests at different axial locations.

X ($I \times J \times K$)	0.125	0.250	0.375	0.500	0.625	0.750	0.875	1.000
$101 \times 62 \times 11$	239.0	239.8	240.6	241.4	241.9	242.1	241.7	210.0
$121 \times 81 \times 21$	235.9	236.7	237.6	238.3	238.9	239.1	238.7	207.6
$141 \times 100 \times 31$	233.4	234.2	235.1	235.8	236.3	236.6	236.1	205.7

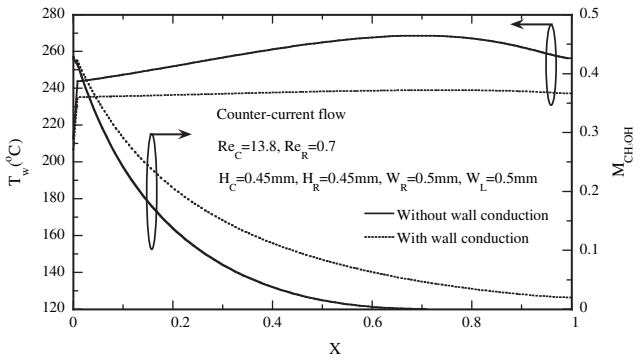

Fig. 3 – Comparisons of the simulation results with and without wall conduction effects for the temperature distributions and CH_3OH mole fraction distributions along the centerline of the channel.

conduction on the thermal development in a micro reformer with combustor are important. It is also found in Fig. 3 that the effects of wall conduction lead to a higher methanol distribution than without a wall conduction effect due to a smaller value of the temperature distribution. However, the wall conduction effects on the heat and mass transport phenomena are remarkable and cannot be neglected in the modeling. Therefore, their effect should be considered in this work.

The influences of the flow configurations on the transport phenomena and the performance of micro reformers are important. To this end, the effects of the flow configurations for co- and counter-current flow on the temperature distributions along different axial location lines and on the local distributions of the mole fractions of various species along the centerline of the reforming channel are presented in Fig. 4. Fig. 4(a) discloses that the temperature distributions are much more uniform due to the shorter thermal entrance length. It is also obvious that a higher temperature distribution is noted for the counter-current flow. This is due to the fact that counter-current flow leads to better thermal management. Fig. 4(b) shows the local distributions of the different species for co- and counter-current flow along the centerline of the reforming channel ($Y = 0.167$). An overall inspection of Fig. 4(b) reveals that both the mole fractions of CH_3OH and H_2O decrease as the fluid moves downstream, while the H_2, CO_2 and CO mole fractions increase with axial location. In addition, a lower CH_3OH mole fraction along the centerline of the channel represents a higher methanol conversion rate. The methanol conversion rate is greater than 91% for the counter-

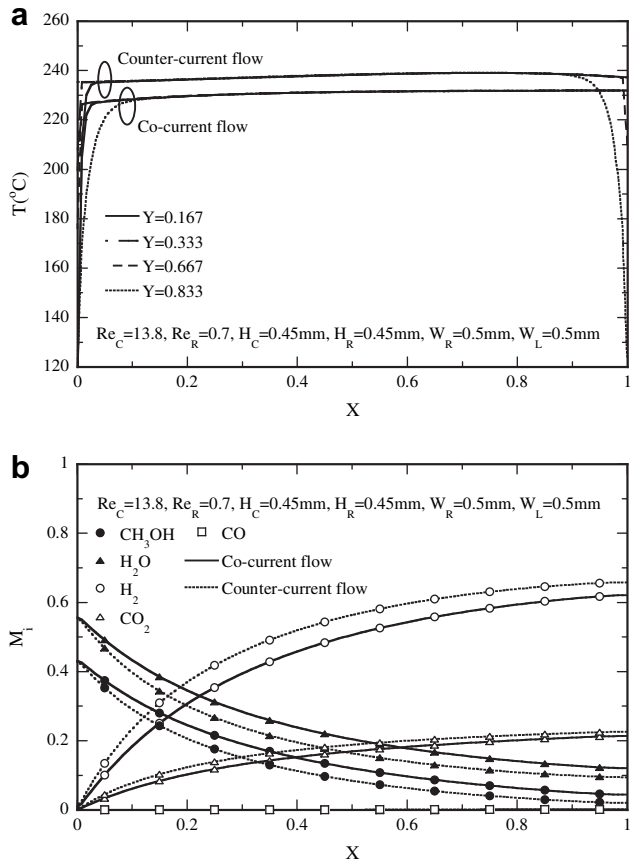

Fig. 4 – Effects of co- and counter-current flow configurations on (a) the temperature distributions along different axial location lines ($Y = 0.333$) and (b) the local distributions of the mole fractions of the various species along the centerline of the reforming channel ($Y = 0.167$).

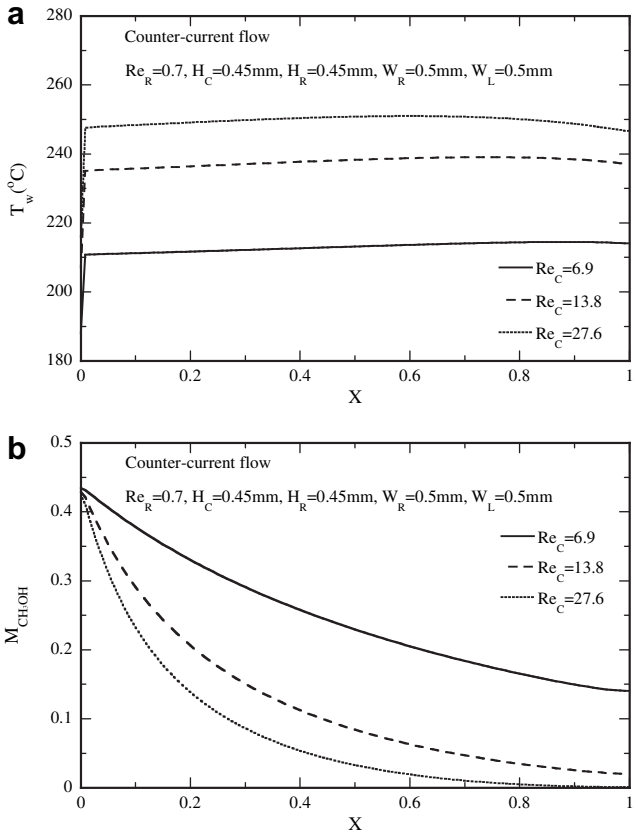

Fig. 5 – Effects of inlet fuel velocities for the combustor on (a) the temperature distributions along the top centerline of the reforming channel ($Y = 0.333$) and (b) the CH_3OH mole fraction distributions along the centerline of the reforming channel ($Y = 0.167$).

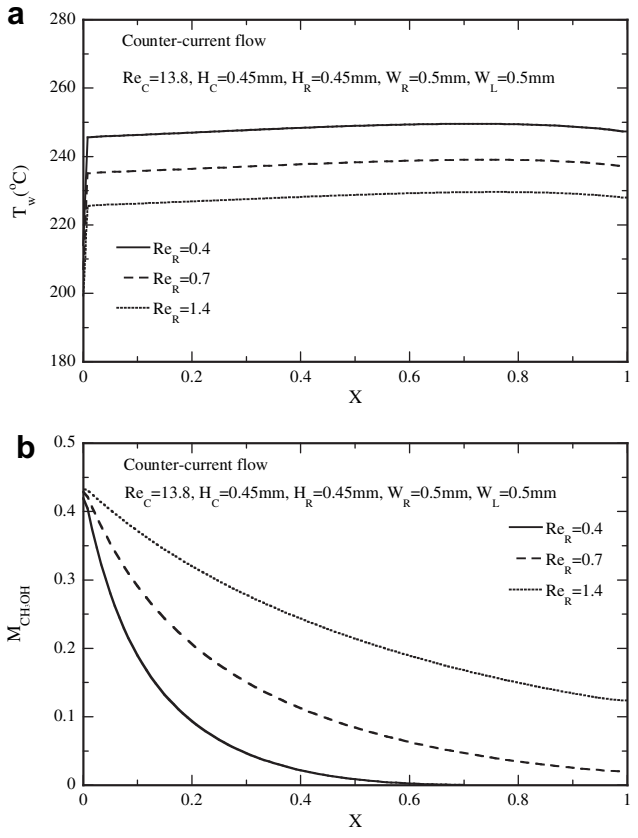

Fig. 6 – Effects of inlet fuel velocities for the reformer on (a) the temperature distributions along the top centerline of the reforming channel (Y = 0.333) and (b) the CH_3OH mole fraction distributions along the centerline of the reforming channel (Y = 0.167).

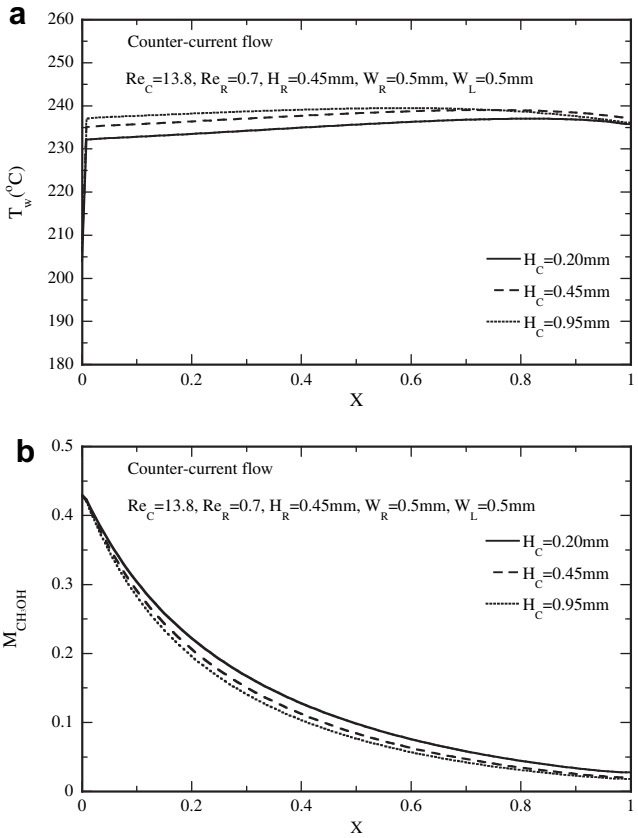

Fig. 7 – Effects of the channel height of the combustor on (a) the temperature distributions along the top centerline of the reforming channel and (b) the CH_3OH mole fraction distributions along the centerline of the reforming channel.

current flow, with a product gas composition of 73.2% H_2, 25.1% CO_2 and 1.7% CO at the outlet of the reforming channel. Comparing co- and counter-current flow via numerical simulation, the results show that the methanol conversion efficiency for counter-current flow could be improved by 10% due to a higher temperature distribution.

In the study of the effects of the Reynolds number (Re) and various geometric parameters on the transport phenomena and micro reformer performance, understanding the detailed distributions of heat and mass transfer is important to the design of a micro reformer with a combustor. The Reynolds number (Re) is one of the key thermo-fluid parameters in the micro reformer and combustor channels which would affect the micro reformer performance. Therefore, effects of the Reynolds number (Re_C) on the combustion channel side on the temperature distributions along the centerline of the top reforming channel ($Y = 0.333$) and CH_3OH mole fraction distributions along the centerline of the reforming channel ($Y = 0.333$) with counter-current flow are examined in Fig. 5. A careful examination of Fig. 5(a) shows that the temperature increases with an increase in the Reynolds number (Re_C) on the combustor side due to a higher inlet flow rate. This is because higher combustion energy is released for a higher inlet flow rate (Reynolds number). Afterwards, an overall inspection of Fig. 5(b) reveals that the CH_3OH mole fractions decrease as the fluid moves downstream due to the reforming chemical reaction. It is also shown that the CH_3OH mole fraction distributions decrease with increasing Reynolds number in the combustor channels. This can be made plausible by noting the fact that the chemical reaction increases as the temperature distributions increase.

Fig. 6 presents the effects of the Reynolds number (Re_R) on the micro reformer side on the temperature distributions along the centerline of the top reforming channel ($Y = 0.333$) and CH_3OH mole fraction distributions along the centerline of the reforming channel ($Y = 0.167$) with counter-current flow. The results in Fig. 6(a) reveal that the temperature distributions are enhanced by the decreased Reynolds number (Re_R) on the micro reformer channels. This is due to a higher Reynolds number (Re_R) significantly increasing the heat leaving the flow channel, which decreases the temperature rise. In addition, it is seen in Fig. 6(b) that the CH_3OH mole fraction distributions decrease with a lower Reynolds number due to a longer time of gas residence and a higher temperature, which results in better methanol conversion.

In order to explain the effectiveness of the geometric parameters for a micro reformer with combustor in thermal management, the temperature and CH_3OH mole fraction

distributions for various geometric parameters were investigated. For a fixed Reynolds number, Fig. 7 demonstrates the effects of the combustion flow channel heights on the temperature distributions along the centerline of the top reforming channel and on the CH_3OH mole fraction distributions along the centerline of the reforming channel with counter-current flow. It is shown in Fig. 7(a) that along the reforming channel, the temperature distributions are very uniform. Overall inspection of Fig. 7(b) disclosed that a lower CH_3OH mole fraction is noted for a system with a greater combustion flow channel height due to a stronger chemical reaction for a higher temperature distribution. This means that a higher efficiency methanol conversion is enhanced via a greater combustion flow channel height.

An exploration of the temperature distributions for various reforming flow channel heights along the centerline of the top reforming channel is presented in Fig. 8(a). For fixed Re, the results show that a higher temperature distribution is found for a micro reformer channel with a lower reforming flow channel height. This is because a higher channel height has a greater hydraulic diameter. As for the effects of reforming flow channel heights on the CH_3OH mole fraction distributions along the centerline of the reforming channel, an overall inspection of Fig. 8(b) reveals that better micro reformer performance is noted for a lower reforming channel height. This implies that the chemical reaction rate is slower for a system with a greater reforming channel height. This seems plausible as a stronger chemical reaction is experienced for a micro reformer channel with a higher wall temperature.

The effects of the channel widths on the temperature distributions and CH_3OH mole fraction distributions for a fixed Reynolds number were also investigated. Fig. 9(a) presents the effects of channel widths on the temperature distributions along the centerline of the top reforming channel ($Y = 0.333$). It is shown in Fig. 9(a) that the local temperature distribution increases with a decrease in the channel width. This may be because a rather narrow channel decreases the heat leaving the flow channel. In Fig. 9(b), the methanol conversion of the micro reformer is slightly enhanced with a wider channel width. It is important to note that a higher temperature distribution will not necessarily provide better methanol conversion, because the channel width increases with increasing catalyst reaction area, which in turn increases the chemical reaction rate.

Fig. 10 shows the effects of the steel widths on the temperature distributions and CH_3OH mole fraction distributions. Fig. 10(a) presents the effects of the steel widths on the temperature distributions along the centerline of the top reforming channel ($Y = 0.333$). Comparison of the

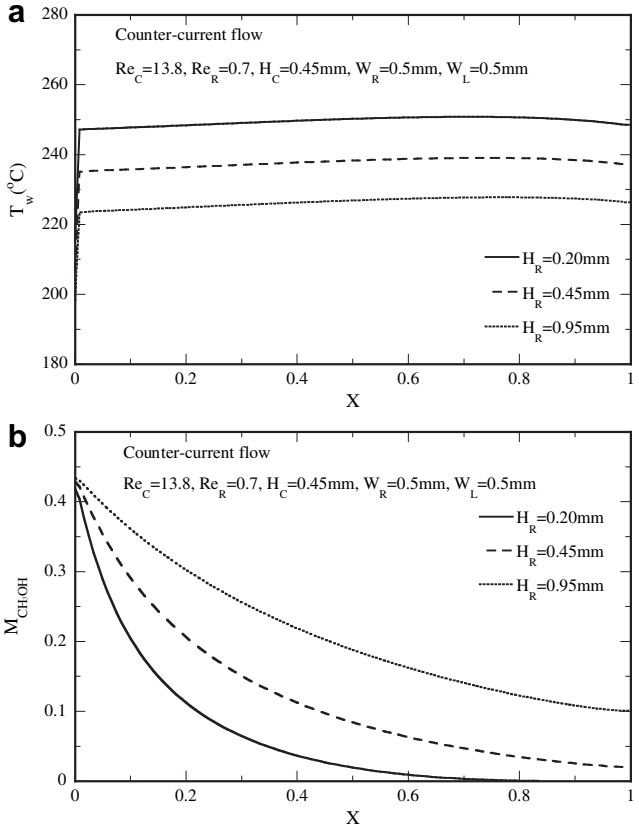

Fig. 8 – Effects of the channel height of the reformer on (a) the temperature distributions along the top centerline of the reforming channel and (b) the CH_3OH mole fraction distributions along the centerline of the reforming channel.

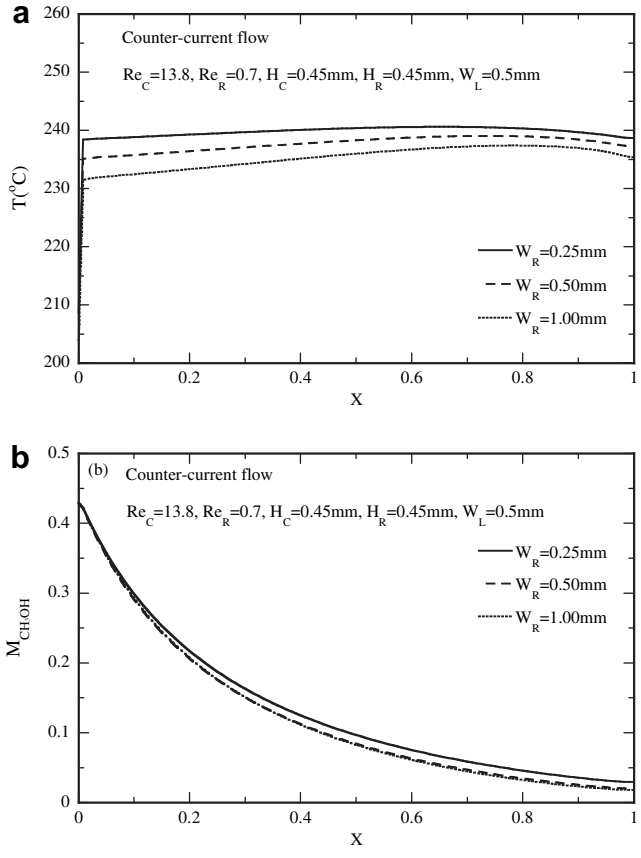

Fig. 9 – Effects of the channel width on (a) the temperature distributions along the top centerline of the reforming channel ($Y = 0.333$) and (b) the CH_3OH mole fraction distributions along the centerline of the reforming channel ($Y = 0.167$).

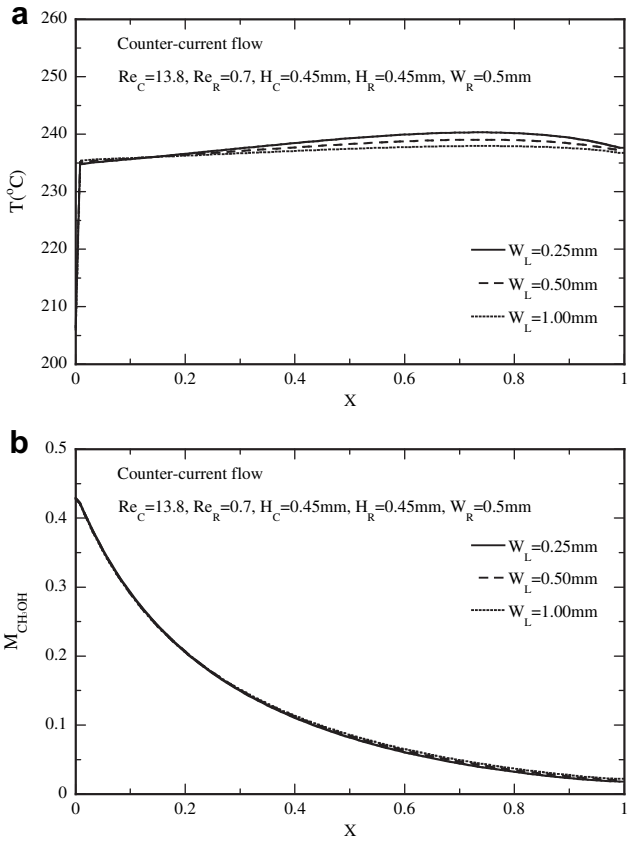

Fig. 10 – Effects of the steel widths on (a) the temperature distributions along the top centerline of the reforming channel (Y = 0.333) and (b) the CH_3OH mole fraction distributions along the centerline of the reforming channel (Y = 0.167).

corresponding curves of the steel widths $W_L = 0.25$ mm, 0.5 mm, and 1.0 mm indicates that a higher temperature distribution is found with wider steel. As for the effects of the steel width on the CH_3OH mole fraction distributions along the centerline of the reforming channel ($Y = 0.167$), the results reveal that they have similar CH_3OH mole fraction distributions. This is due to having similar temperature distributions. Therefore, the steel width does not have a significant impact on the methanol conversion.

Fig. 11 demonstrates the effects of the Reynolds number (Re_C) for the combustor on methanol conversion and wall temperature of the reforming channel in the plate methanol steam micro reformer. For comparison, the results without the wall conduction effect in the model are also presented. An overall inspection of Fig. 11 shows that the wall temperature increases with increase of the Reynolds number (Re_C) on the combustion channel side. This is plausible because the inlet fuel velocity increases in the channel as the Reynolds number increases. As for the methanol conversion, the results show that the methanol conversion increases as the Reynolds number of the combustion channel increases, which in turn increases the wall temperature. In addition, the wall conduction effect is also shown in Fig. 11. The deviations in

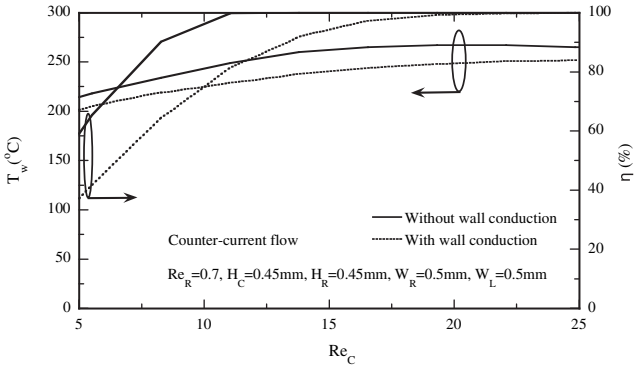

Fig. 11 – Effects of the Reynolds number (Re) of the combustor on wall temperature and methanol conversion.

methanol conversion between the results with and without consideration of wall conduction effects are larger. This means that the wall conduction effect on methanol conversion and wall temperature become significant and cannot be neglected in the modeling.

5. Conclusions

With an appropriate design of the flow configurations in the reactor, the thermal management of a micro reformer with combustor can be achieved efficiently. To reach this end, various flow configurations for co- and counter-current flow have been proposed. In addition, the effects of the Reynolds number and various geometric parameters have also been investigated by using numerical simulations of the detailed gas transport phenomena and micro reformer performance. What follows are the major findings.

(1) The deviations between the predictions with and without consideration of the wall conduction effects reveal the influences of the wall conduction on the transport phenomena and the performance of the micro reformer. The present results provide evidence for the significance of a wall conduction effect and imply that it is necessary to include this effect in modeling and analysis.
(2) The application of the flow configuration design in a plate methanol steam micro reformer with methanol catalytic combustor leads to improved thermal management and micro reformer performance. The effects can be enhanced with a counter-current flow configuration in a plate methanol steam micro reformer with methanol catalytic combustor.
(3) With a higher Reynolds number on the combustor side, the wall temperature is increased and methanol conversion can thus be enhanced. Meanwhile, a reduced Reynolds number for the reactant gas on the micro reformer side will raise the reactant gas residence time, which in turn increases the methanol conversion and improves the temperature distributions.
(4) The effects of channel geometry have a significant impact on the methanol conversion and heat and mass transfer in

the plate methanol micro reformer with methanol catalytic combustor.

Acknowledgement

The study was supported by the National Science Council, the Republic of China, through the grants NSC 97-2221-E-211-015-MY2.

REFERENCES

[1] Holladay JD, Wang Y, Jones E. Review of developments in portable hydrogen production using microreactor technology. Chem. Rev. 2004;104:4767–90.
[2] Pfeifer P, Schubert K, Liauw MA, Emig G. Electrically heated microreactors for methanol steam reforming. Chem. Eng. Res. Des. 2003;81(7):711–20.
[3] Park GG, Seo DJ, Park SH, Yoon YG, Kim CS, Yoon WL. Development of microchannel methanol steam reformer. Chem. Eng. J. 2004;101(1):87–92.
[4] Lim MS, Kim MR, Noh J, Woo SI. A plate-type reactor coated with zirconia-sol and catalyst mixture for methanol steam-reforming. J. Power Sources 2005;140(1):66–71.
[5] Kundu A, Jang JH, Lee HR, Kim SH, Gil JH, Jung CR, et al. MEMS-based micro-fuel processor for application in a cell phone. J. Power Sources 2006;162(1):572–8.
[6] Kwon OJ, Hwang SM, Ahn JG, Kim JJ. Silicon-based miniaturized-reformer for portable fuel cell applications. J. Power Sources 2006;156(2):253–9.
[7] Ha JW, Jang JH, Gil JH, Kim SH. The fabrication and performance of a poly(dimethylsiloxane) (PDMS)-based microreformer for application to electronics. Int. J. Hydrogen Energy 2008;33(8):2059–63.
[8] Kwon OJ, Yoon DH, Kim JJ. Silicon-based miniaturized reformer with methanol catalytic burner. Chem. Eng. J. 2008; 140(1):466–72.
[9] Sohn JM, Byun YC, Cho JY, Choe J, Song KH. Development of the integrated methanol fuel processor using micro-channel patterned devices and its performance for steam reforming of methanol. Int. J. Hydrogen Energy 2007;32(18): 5103–8.
[10] Won JY, Jun HK, Jeon MK, Woo SI. Performance of microchannel reactor combined with combustor for methanol steam reforming. Catal. Today 2006;111(3): 158–63.
[11] Kim T. Micro methanol reformer combined with a catalytic combustor for a PEM fuel cell. Int. J. Hydrogen Energy 2009;34 (16):6790–8.
[12] Park DE, Kim T, Kwon S, Kim CK, Yoon E. Micromachined methanol steam reforming system as a hydrogen supplier for portable proton exchange membrane fuel cells. Sens. Actuators A 2007;135(1):58–66.
[13] Yoshida K, Tanaka S, Hiraki H, Esashi M. A micro fuel reformer integrated with a combustor and a microchannel evaporator. J. Micromech. Microeng. 2006;16:191–7.
[14] Park GG, Yim SD, Yoon YG, Kim CS, Seo DJ, Eguchi K. Hydrogen production with integrated microchannel fuel processor using methanol for portable fuel cell systems. Catal. Today 2005;110(1–2):108–13.
[15] Park GG, Yim SD, Yoon YG, Lee WY, Kim WS, Seo DJ, et al. Hydrogen production with integrated microchannel fuel processor for portable fuel cell systems. J. Power Sources 2005;145(2):702–6.
[16] Kwon OJ, Hwang SM, Chae JH, Kang MS, Kim JJ. Performance of a miniaturized silicon reformer-PrOx-fuel cell system. J. Power Sources 2007;165(1):342–6.
[17] Kim T, Kwon S. MEMS fuel cell system integrated with a methanol reformer for a portable power source. Sens. Actuators A 2009;154(2):204–11.
[18] Suh JS, Lee MT, Greif R, Grigoropoulos CP. A study of steam methanol reforming in a microreactor. J. Power Sources 2007; 173(1):458–66.
[19] Suh JS, Lee MT, Greif R, Grigoropoulos CP. Transport phenomena in a steam-methanol reforming microreactor with internal heating. Int. J. Hydrogen Energy 2009;34(1):314–22.
[20] Karim A, Bravo J, Datye A. Nonisothermality in packed bed reactors for steam reforming of methanol. Appl. Catal. A 2005;282(1):101–9.
[21] Karim A, Bravo J, Gorm D, Conant T, Datye A. Comparison of wall-coated and packed-bed reactors for steam reforming of methanol. Catal. Today 2005;110(1):86–91.
[22] Cao C, Wang Y, Holladay JD, Jones EO, Palo DR. Design of micro-scale fuel processors assisted by numerical modeling. AlChE J. 2005;51(3):982–8.
[23] Pattekar AV, Kothare MV. A radial microfluidic fuel processor. J. Power Sources 2005;147(1–2):116–27.
[24] Pattekar AV, Kothare MV. A microreactor for hydrogen production in micro fuel cell applications. J. Microelectromech. Syst. 2004;13(1):7–18.
[25] Park HG, Malen JA, Piggott III WT, Morse JD, Greif R, Grigoropoulos CP. Methanol steam reformer on a silicon wafer. J. Microelectromech. Syst. 2006;15(4):976–85.
[26] Kawamura Y, Ogura N, Yamamoto T, Igarashi A. A miniaturized methanol reformer with Si-based microreactor for a small PEMFC. Chem. Eng. Sci. 2006;61(4):1092–101.
[27] Hsueh CY, Chu HS, Yan WM. Numerical study on micro-reformer performance and local transport phenomena of the plate methanol steam micro-reformer. J. Power Sources 2009; 187(2):535–43.
[28] Chen F, Chang MH, Kuo CY, Hsueh CY, Yan WM. Analysis of a plate-type microreformer for methanol steam reforming reaction. Energy Fuels 2009;23(10):5092–8.
[29] Kim T, Kwon S. Design, fabrication and testing of a catalytic microreactor for hydrogen production. J. Micromech. Microeng. 2006;16(1):1760–8.
[30] Deshmukh SR, Vlachos DG. Effect of flow configuration on the operation of coupled combustor/reformer microdevices for hydrogen production. Chem. Eng. Sci. 2005;60(21):5718–28.
[31] Deshmukh SR, Vlachos DG. CFD simulations of coupled, countercurrent combustor/reformer microdevices for hydrogen production. Ind. Eng. Chem. Res. 2005;44(14): 4982–92.
[32] Arzamendi G, Dieguez PM, Montes M, Centeno MA, Odriozola JA, Gandia LM. Integration of methanol steam reforming and combustion in a microchannel reactor for H_2 production: a CFD simulation study. Catal. Today 2009;143 (1–2):25–31.
[33] Arzamendi G, Dieguez PM, Montes M, Odriozola JA, Sousa-Aguiar EF, Gandia LM. Methane steam reforming in a microchannel reactor for GTL intensification: a computational fluid dynamics simulation study. Chem. Eng. Sci. 2009;154(1–3):168–73.
[34] Pan L, Wang S. Modeling of a compact plate-fin reformer for methanol steam reforming in fuel cell systems. Chem. Eng. J. 2005;108(1):51–8.
[35] Zanfir M, Gavriilidis A. Catalytic combustion assisted methane steam reforming in a catalytic plate reactor. Chem. Eng. Sci. 2003;58(17):3947–60.
[36] Varesano A, Guaglio I, Saracco G, Maffettone PL. Dynamics of a methanol reformer for automotive applications. Ind. Eng. Chem. Res. 2005;44(4):759–68.

[37] White FM. Viscous fluid flow. 2nd ed. McGraw-Hill; 1991.
[38] Ergun S. Fluid flow through packed columns. Chem. Eng. Prog. 1952;48(2):89–94.
[39] Pepply A, Amphlett JC, Kearns LM, Mann RF. Methanol steam reforming on $Cu/ZnO/Al_2O_3$ catalysts. Part 2. A comprehensive kinetic model. Appl. Catal. A 1999;179(1–2): 31–49.
[40] Mastalir A, Frank B, Szizybalski A, Soerijanto H, Deshpande A, Niederberger M, et al. Steam reforming of methanol over $Cu/ZrO_2/CeO_2$ catalysts: a kinetic study. J. Catal. 2005;230(2):464–75.
[41] Pasel J, Emonts B, Peters R, Stolten D. A structured test reactor for the evaporation of methanol on the basis of a catalytic combustion. Catal. Today 2001;69(1–4):193–200.